GEONICS LIMITED
1745 Meyerside Dr. Unit 8 Mississauga, Ontario Canada L5T 1C6

Tel: (905) 670-9580
Fax: (905) 670-9204
E-mail: geonics@geonics.com
URL:http//www.geonics.com

Technical Note TN-32

Application of TDEM Techniques to Metal Detection and Discrimination: A Case History with the New Geonics EM-63 Fully Time-Domain Metal Detector.

J.D. McNeill, M. Bosnar

April, 2000.

Geonics Limited Technical Note TN-32

Application of TDEM Techniques to Metal Detection and Discrimination: A Case History with the New Geonics EM-63 Fully Time-Domain Metal Detector.

Introduction

In this technical note we first examine some of the major advantages of using TDEM techniques for the detection and identification of buried metallic targets. We then present data from a TDEM survey over various metallic targets at the University of Waterloo "Columbia Test Site", using the new fully time-domain, Geonics EM-63 metal detector, to illustrate these advantages.

Background

It is by now well established that, although the use of magnetometers permits detection of ferrous metallic objects at the greatest depths, the real problem is generally not detection at great depths, but rather identification of the target itself. In typical UXO surveys, for example, the number of unexploded targets can be an extremely small fraction (less than one percent) of the total number of detected targets. It is clearly not economical to dig up all detected targets, and there thus is a vital requirement for a technique that helps to separate UXO from scrap metal. The only geophysical techniques that offer promise for this degree of discrimination are inductive ground electromagnetic techniques and ground penetrating radar (GPR). To date GPR has not been, for a variety or reasons, particularly useful for UXO detection and identification, and it is clear that inductive electromagnetic techniques are the leading contender to help solve this difficult problem.

The next question concerns whether operation in the time or frequency-domain is most advantageous for this application. In Geonics Limited Technical Note TN-30 "Why Doesn't Geonics Limited Build a Multi-frequency EM31 or EM38" it was noted that although the EM31 and EM38 were both widely used for metal detection, Geonics Limited did not pursue the "metal detection application" for these instruments. We realized that target interpretation (including even the simple act of accurately locating the target) could prove to be very difficult with a frequency-domain instrument in which the transmitter and receiver coils are significantly separated in terms of distance to a target.

The principle reason for this difficulty lies in the fact that many ferrous metallic targets are either plate-like or rod-like in their shape, which has a very significant effect on their response to EM excitation. For the following discussion we will assume that the target is plate-like, but similar response features are found in targets exhibiting cylindrical symmetry.

When a horizontal, plate-like, ferrous target is energized by a vertical electromagnetic dipole located above its center, the primary magnetic field is perpendicular to the surface of the plate, and the electromagnetic response arises principally from eddy current flow in the plate. In the frequency-domain the magnitude and phase of this response are determined by the conductivity and permeability of the plate, as well as by all three of its dimensions. These same factors determine the magnitude and shape of the time-domain decay response. Much is known about the nature of this response in either the frequency or time-domain.

What is not so well known is that when the same ferrous plate is energized by a dipole located so that the primary magnetic field is essentially parallel rather than perpendicular to either long dimension of the plate, a substantial response is also excited. The magnitude of this response (which we call the permeability response) is of the same order of magnitude as the eddy current response. The reason for this response is that orientation of the primary magnetic field parallel to the long plate dimension effectively polarizes the magnetic dipoles in the plate. Rapid removal of the primary field (in the time-domain) allows the oriented magnetic dipoles to relax to their normal random orientation, but the relaxation occurs relatively slowly, with decay characteristics completely unlike those from an eddy current response. Just how this time-relaxation response depends on the various plate parameters is poorly understood. In the frequency-domain, the result of this effect is that the frequency-dependence of the magnitude and phase of the secondary magnetic field from this excitation will be quite unlike that which arises from eddy current flow.

This effect will, of course, also be present to a limited extent when the energizing dipole is located above the center of the sheet, but for this geometry the eddy current response completely dominates. Similarly, when the primary magnetic field is parallel to the sheet, a very small eddy current response will arise, but for this geometry the permeability response will completely dominate.

Readers who are interested in learning more about this effect, particularly with respect to typical UXO targets, are referred to the accompanying paper "Application of Time-domain Electromagnetic Techniques to UXO Detection" by McNeill and Bosnar (Proceedings UXO Forum, 1996)

In the most general case of a ferrous target having the approximate shape of a three-dimensional prism, we can expect a rather complicated combination of both "eddy current" response and "permeability" response for primary field excitation along each of the three axes, with the relative amount of each response depending on the relative dimensions of the quasi-prismatic target.

Now a problem arises when we try to characterize such a target using a dipole-dipole electromagnetic system in which the intercoil-spacing is of the same order of magnitude or larger than the distance of the system from the target. In this case it is quite possible for the transmitter to be located so that it is largely energizing eddy current response, whereas the receiver can be located so that it is responding largely to permeability

response, or vice-versa. More often, the transmitter and receiver locations will be such that both responses are energized and detected.

It was evident that, since target orientation is arbitrary, use of dipole-dipole systems with intercoil-spacing of the order of depth to target could lead to difficulty in the interpretation of survey data, as was often seen in actual practice. It is therefore our contention that there is a significant advantage to be derived from using a superimposed, dipole-dipole EM system.

Advantages of Time-Domain Operation

The discussion above suggests that an electromagnetic system in which both transmitter and receiver coils are essentially superimposed will result in a simplified spatial response. This is most easily done in the time-domain, where, at least in principle, measurement of target response is made in the absence of the primary magnetic field, and variations in the transmitter/receiver coupling have minimal effect.

There are further advantages to operation in the time-domain. The larger ferrous targets that are often the object of UXO surveys have the most diagnostic portion of their response either at very late times (McNeill and Bosnar, enclosed) or at very low frequencies, where, in either case, the signals are extremely small. To measure accurately these small signals requires an excellent signal-to-noise ratio (SNR), which, contrary to popular opinion, is easily obtained in the time-domain. It is widely believed that operation in the frequency-domain is by far the more noise-free, since in a frequency-domain system the synchronous detection gates are wide, whereas many of the gates in a time-domain system are, by design, quite narrow. Nevertheless the late-time gates of a time-domain system are almost as wide as those of a frequency-domain system, and thus the signal-to-noise ratio for these gates is almost the same. It is true that the earlier time gates are much narrower, but this is of no consequence since at earlier time the received signal is also orders of magnitude larger, with excellent signal-to-noise ratio regardless of narrow gates. The principle reason that frequency-domain systems appear to have higher signal-to-noise ratio is that they generally operate at much higher base frequencies, and thus have more cycles over which to integrate, at the expense, however, of loosing useful low-frequency information.

Moreover, when operating at the very low base frequencies that are necessary to characterize large UXO targets, a principle source of noise is motion of the system in the earth's magnetic field. The only way to reduce this noise is to employ a very large transmitter dipole moment, much more easily achieved in the time-domain.

Finally the response from large, deep targets is spatially diffuse, requiring good control of the instrument zero level to detect and measure these small, spatially slowly-varying signals. In the frequency-domain, measurement of the small secondary signal is always made in the presence of the much larger primary magnetic field. Small variations in the primary field therefore result in large errors in the secondary field. For this reason,

various techniques have been employed over the years to "buck out" this troublesome primary field. Such techniques work reasonably well for airborne electromagnetic systems, however their implementation becomes more difficult for multi-frequency ground systems, particularly those in which the transmitter and receiver coils are physically close to each other and are thus electrically "closely-coupled". The reason is that the residual null signal remaining after the "bucking" is caused largely by poorly understood electrostatic effects, which vary both with frequency and, often, with the (spatially varying) properties of the ground in the vicinity of the system coils. Controlling these effects to produce a stable zero-level for each frequency can be extremely difficult.

Operation in the time-domain also has problems (it is difficult to completely terminate the primary magnetic field in a very short time) however they are simpler to deal with and, furthermore, are independent of the ground characteristics.

Case History, University of Waterloo "Columbia Test Site"

A plan view of the survey site is shown in Figure 1, which indicates the nature of the various buried targets and the direction of the EM-63 survey lines. The miscellaneous metallic targets numbered from 1 to 9 are described in Table 1 below. These targets were placed on the surface.

TABLE 1

Miscellaneous Metallic Targets

Item	Description
1	Aluminum ball, 10 cm diameter
2	Steel ball, 10 cm diameter
3	Steel ball, 9 cm diameter
4	Aluminum plate, 50x50 cm, 1.6 mm thick
5	Aluminum plate, 30x25 cm, 1.6 mm thick
6	Steel plate, 20x40 cm, 1.6 mm thick
7	Steel plate, 25x25 cm, 1.6 mm thick
8	Inert 105 mm projectile, long axis perpendicular to survey line
9	Inert 105 mm projectile, long axis parallel to survey line

Targets 1-3 were chosen to illustrate the differences between ferrous and non-ferrous materials with spherical symmetry. Targets 4-7 approximate ferrous and non-ferrous scrap metal. UXO targets 8-9 are chosen to illustrate various effects discussed below.

Figure 2 shows the responses measured over virtually the entire survey area, at a gate time centered at approximately 180 μ sec. There are several points to note.

1. The amplitude scale is not linear, the reason being that the dynamic range of TDEM signals is so large that compression is necessary; in this case it is the square root of the amplitudes which are plotted, as indicated on the coloured scale bar

2. At this relatively early time gate all targets are clearly indicated (although the most deeply buried pipe does not show a strong signature at this time). Furthermore the orientation and/or aspect ratio of the larger targets is also clearly indicated.

3. The signal-to-noise ratio is excellent over the whole survey area. It is most probable that the few small responses not related to known targets are due to scrap metal left at the site by previous experimenters.

Figure 3 shows similar data, but now at a time gate of approximately 13.2 msec. The only targets still visible are the shallow 8 m long pipe, and the two 105 mm projectiles, illustrating the usefulness of late-time TDEM measurements for resolving sub-surface targets on the basis of their time decay responses.

There is always a problem with plotting the multi-parameter data that is generated from multi-frequency FDEM or multi-time TDEM data. A simple approach to this problem is shown in Figure 4. In this case an approximate time constant for each anomaly has been calculated from the complete time-decay curve. As we shall see below, the time decay responses are rarely simple exponentials, so computation of an apparent time-constant involves an approximation over at least part of the time-decay curve. Nevertheless an apparent time-constant yields a one-parameter summary of the complete curve which can be very useful, as shown in Figure 4, where the vertical coloured scale bar now represents the apparent time-constant in μ sec. We see that all barrels, regardless of their depth of burial or indeed whether they occur singly or in groups, show essentially the same apparent time-constant as long as there is sufficient SNR to make an accurate calculation (the most deeply buried single drum is an exception). Likewise the pipes and plates exhibit their own representative apparent time-constants. On the other hand, the nine metallic objects sitting on the surface show a variety of apparent time-constants, the two 105 mm projectiles being similar to each other, and generally distinct from the other small objects.

Figure 5 shows the detailed time decay for each of the three drums, buried at different depths. Although at first sight the three responses seem to be different, shifting the responses vertically with respect to each other confirms that the three curves are virtually identical and thus that the time decay response is independent of the depth of burial. At late times, the three curves are exhibiting exponential behavior (note that the plots are log-log) as would be expected from the fact that, although they are made of ferrous metal, the metal is thin and the late-time response is due entirely to eddy current flow.

Figure 6 shows the time decays measured near each of the two groups of buried drums. The shape of these curves is essentially the same as those of Figure 5, showing that

the response from multiple drums, even in close proximity to one another, is nearly the same as the response from a single drum. Such a result is not unexpected since the combined late-time decay response from two similar objects in close proximity to each other changes very little until the two objects are virtually in physical contact. The early time response is more likely to show some effect from mutual coupling, as is seen in the figure.

Figure 7 shows the time decays measured over two of the three buried pipes (the response over the deepest pipe was too small to measure accurately). Once again the shapes of the responses are independent of depth. In this case the responses do not become exponential since the eddy currents continue to diffuse with time slowly down the length of the pipe. The response from a long pipe is very different from that from a relatively compact drum.

Figure 8 shows the response measured both over the center of a large steel plate (curve A) and off the edge of the same plate (curve B). In the first case the response is entirely due to eddy current flow, in the second we see only permeability response since the primary magnetic field is now parallel with the long dimension of the plate. The two responses are completely different, the eddy current response becoming exponential at late time whereas the permeability response shows a slowly varying power-law response throughout the whole measurement time. Furthermore, at early time the eddy current response is by far the larger of the two, however at late time the permeability response dominates, as a result of the slower power-law decay rate.

We now turn our attention to target spatial responses. Figure 9 shows a spatial profile (horizontal axis is distance down the survey line in meters) over the first eight of the surface metallic targets of Table 1, measured over a wide range of time. Once again the dynamic range exhibited by the targets is enormous so that it is necessary to plot the amplitudes of the various responses in small groups, using different scales at different times. Thus the scale is 0-4000 mv for time channels 1 through 5, 0-2000 for channels 6 through 10, etc. The uppermost plot is the integrated response that would be measured by the single gate of the Geonics EM 61 TDEM metal detector. These plots show a great variety of responses, from those that start large and stay large, through to those that start large but decay quickly and finally to those that start small but persist to late times.

It is not apparent from Figure 9 (where the horizontal scale is compressed due to plotting all target responses on a single page), but is obvious from Fig. 12 of McNeill and Bosnar (enclosed) that the spatial responses from aluminum targets and steel plates are quite different for the reasons outlined above. The spatial responses, provided that they are measured at sufficiently high spatial resolution, provide additional diagnostic information as to target geometry and metallic type.

Returning to time responses, Figure 10 shows measurements made directly over the top of each of the eight surface targets. Some responses show exponential decay at late times, with different time constants; others show extended times over which the

response is accurately power-law, with different values of exponent; some show combinations of both responses. All are useful for distinguishing between ferrous and non-ferrous metals, and for indicating the relative size of different targets.

Finally, Figure 11 shows the time response of a 105 mm projectile measured directly over the top, and, in addition, a short lateral distance in the direction of the long axis. The figure clearly demonstrates the difference in time decays when, in the first case, eddy currents are dominant and, in the second, permeability effects control the response.

Conclusions

It is shown in this technical note that the combination of (1) the highly resolved spatial response resulting from use of superimposed coils, and (2) highly accurate time decay data, measured to very late times with a powerful transmitter, is instrumental in distinguishing the time-domain responses of various types of UXO, as well as discriminating UXO from scrap metal.

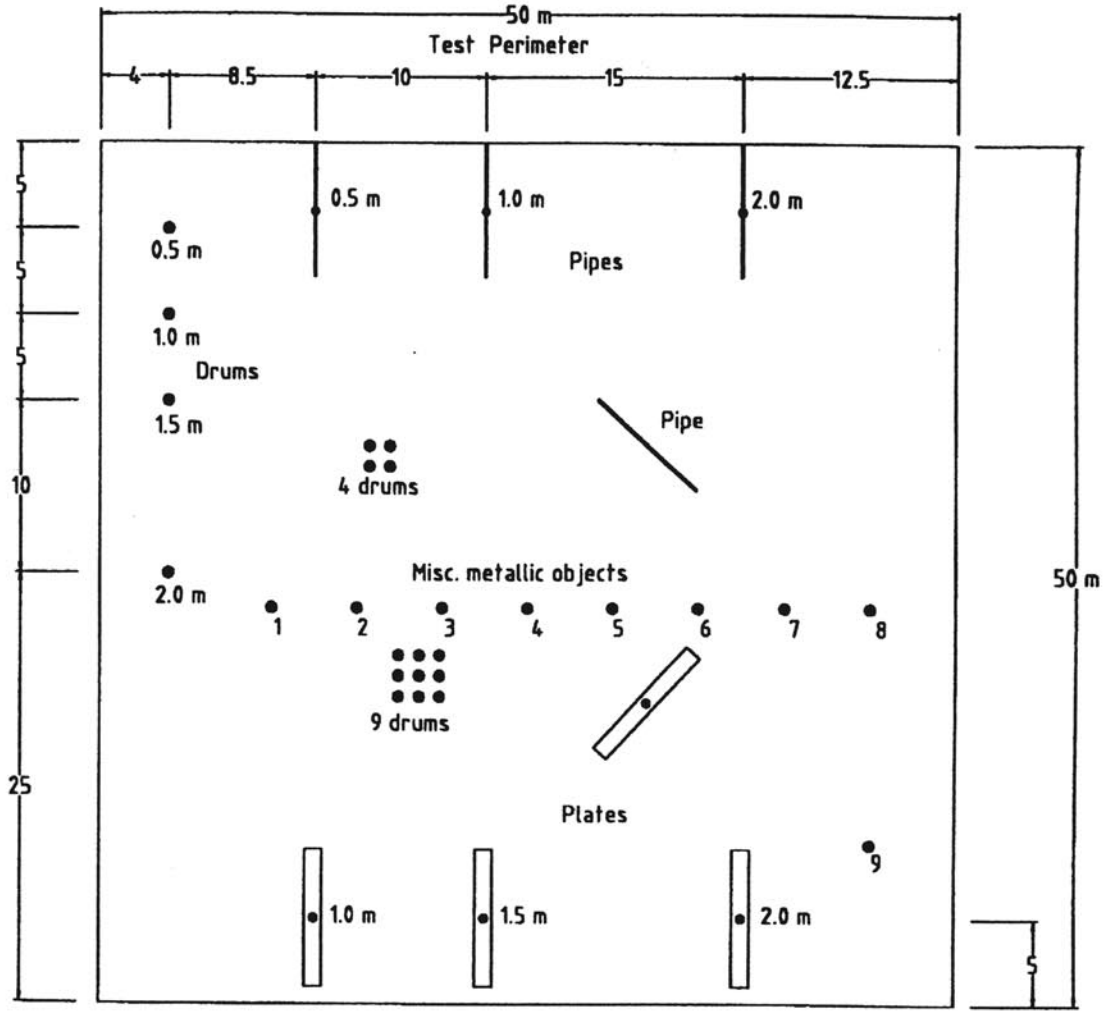

COLUMBIA GOLF COURSE TEST SITE

vertical barrel .6 by .9 m ●

pipeline .10 by 8 m ——

sheet metal 1 by 8 m ▭

target markers with depth •

All items buried except 1-8&9, which are on the surface

Survey direction ⟷

Figure 1

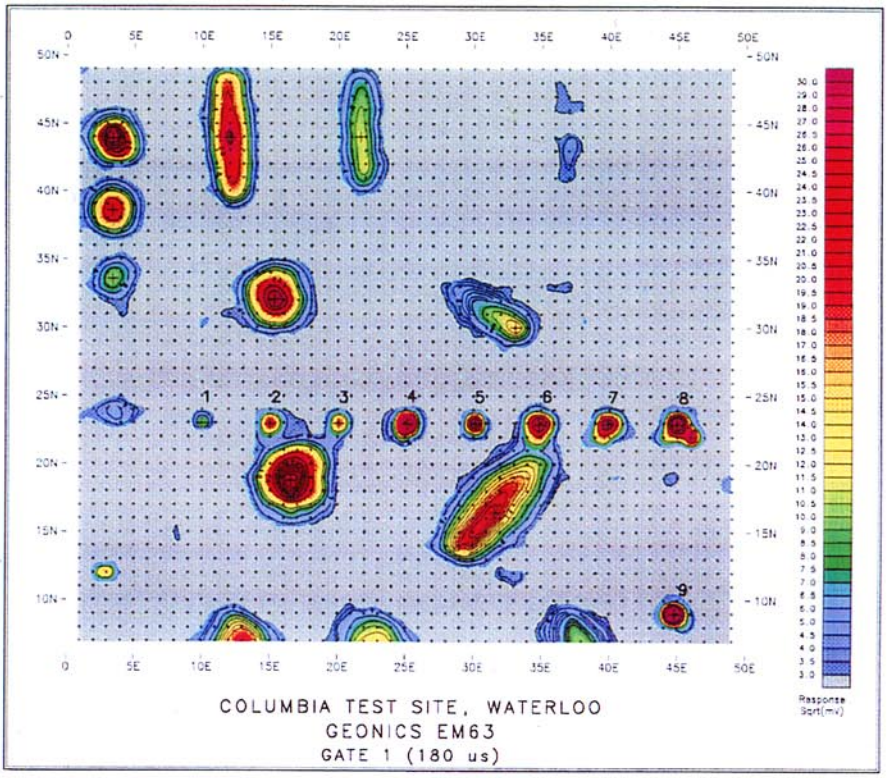

Figure 2

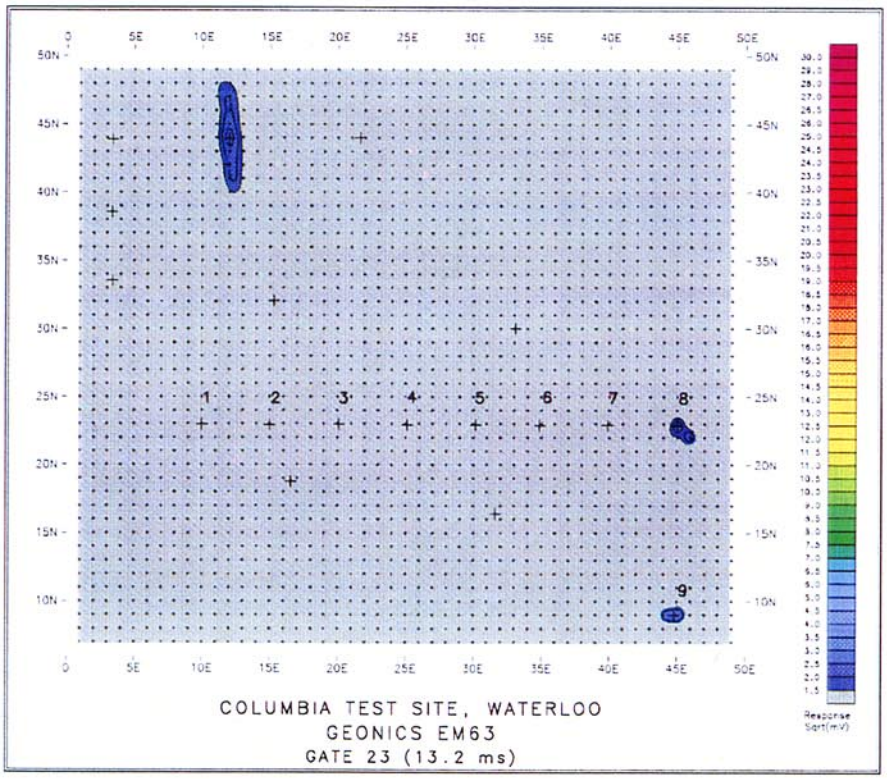

Figure 3

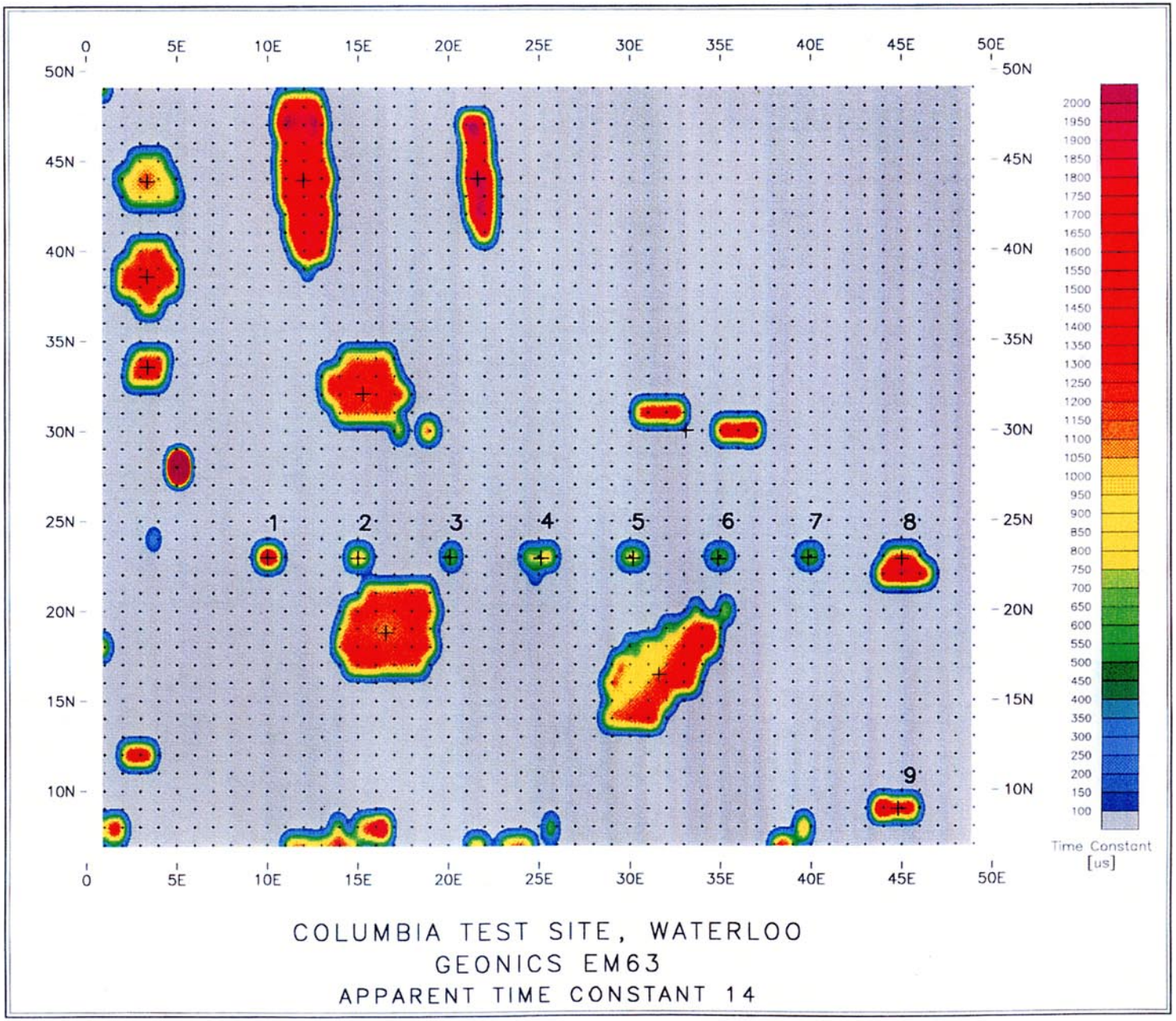
0
5E
10E
15E
20E
25E
30E
35E
40E
45E
50E
50N
45N
40N
35N
30N
25N
20N
15N
10N
1
2
3
4
5
6
7
8
9
2000
1950
1900
1850
1800
1750
1700
1650
1600
1550
1500
1450
1400
1350
1300
1250
1200
1150
1100
1050
1000
950
900
850
800
750
700
650
600
550
500
450
400
350
300
250
200
150
100
Time Constant
[us]
COLUMBIA TEST SITE, WATERLOO
GEONICS EM63
APPARENT TIME CONSTANT 14

Figure 4

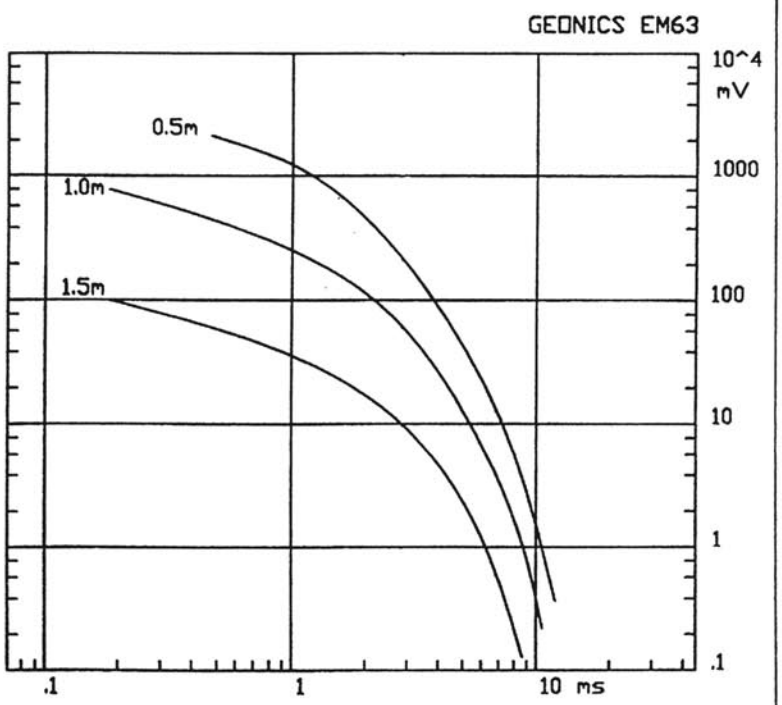

Single drum at 0.5, 1 & 1.5 meter depth

Figure 5

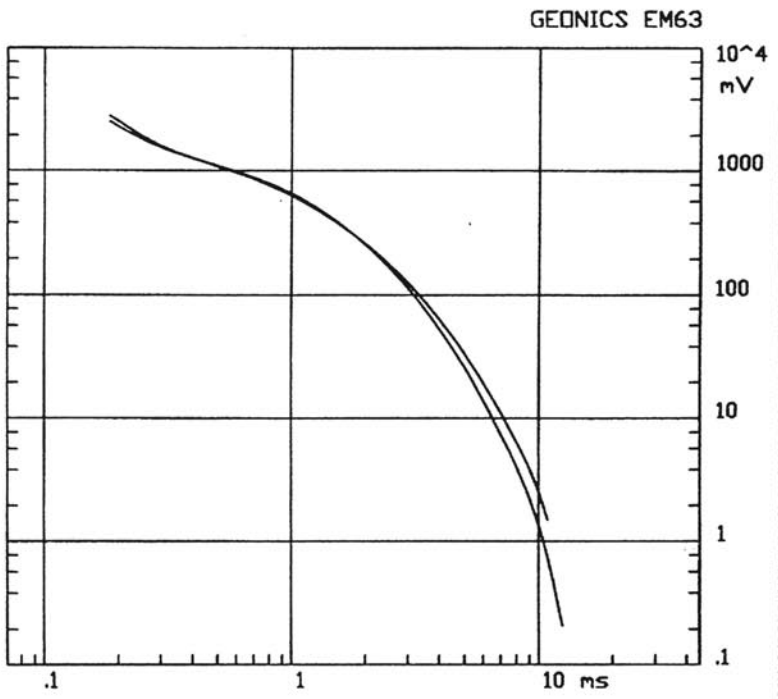

Multiple drums (9) & (4) at 1m depth

Figure 6

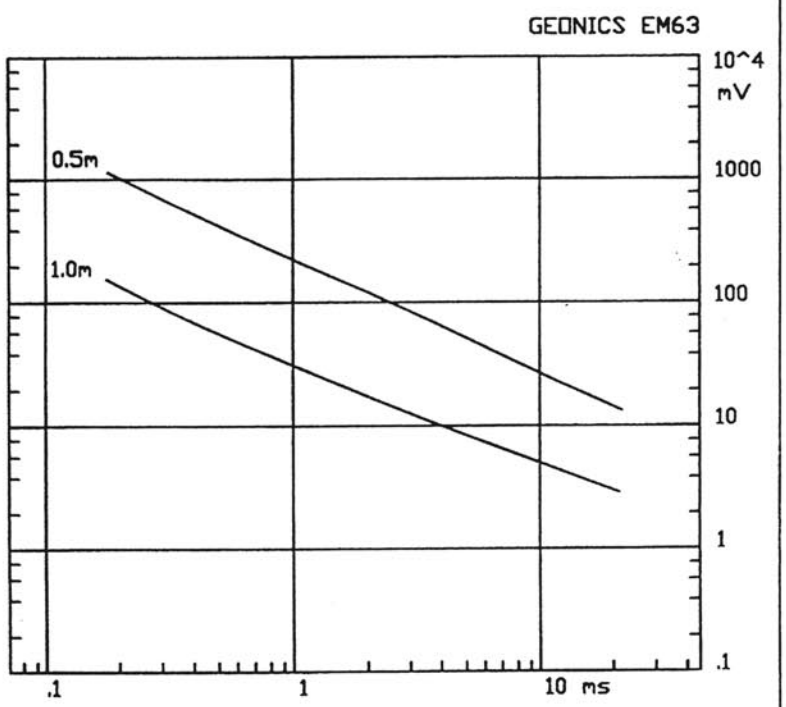

Steel pipes .1m dia x 8m

Figure 7

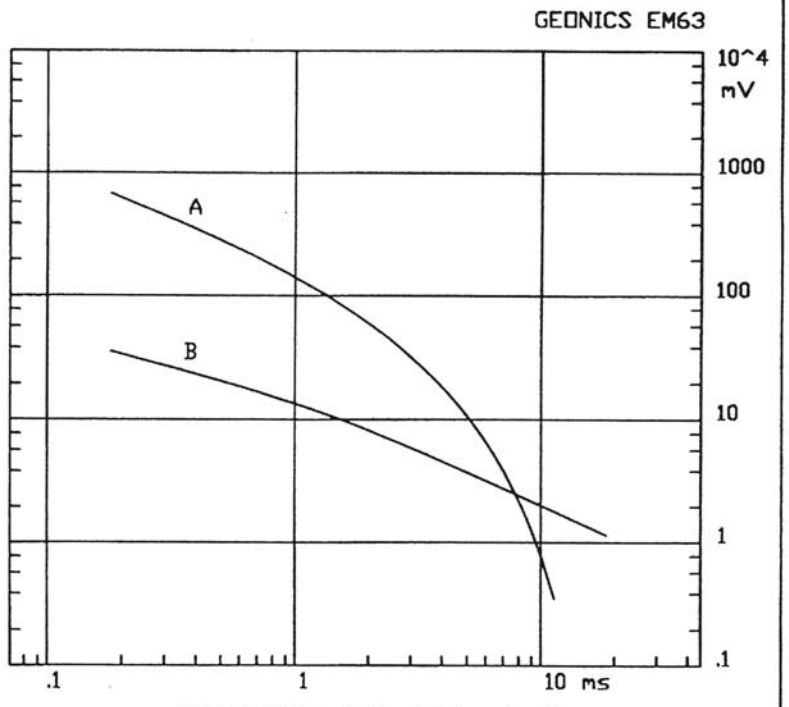

Steel plate 1x8m at 1m depth

Figure 8

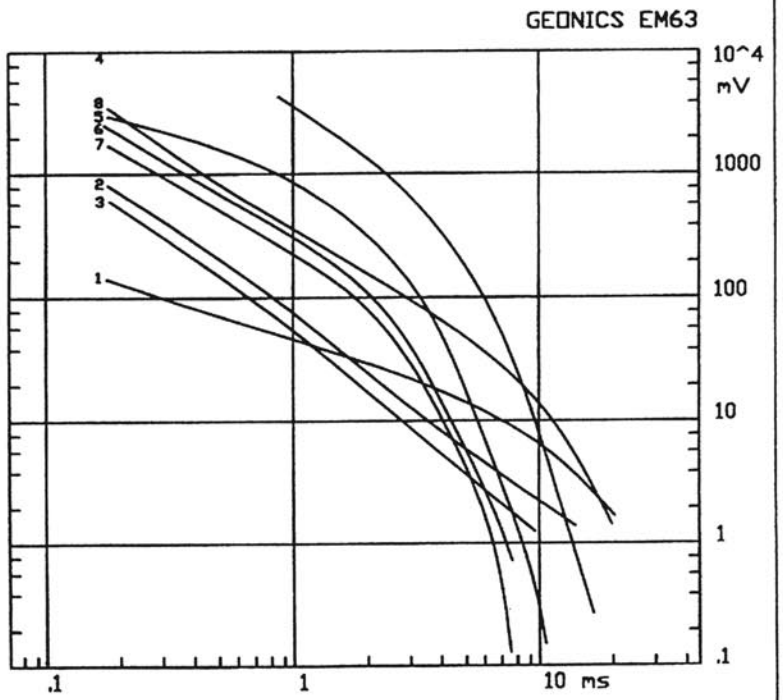

Different metalic targets on surface

Figure 10

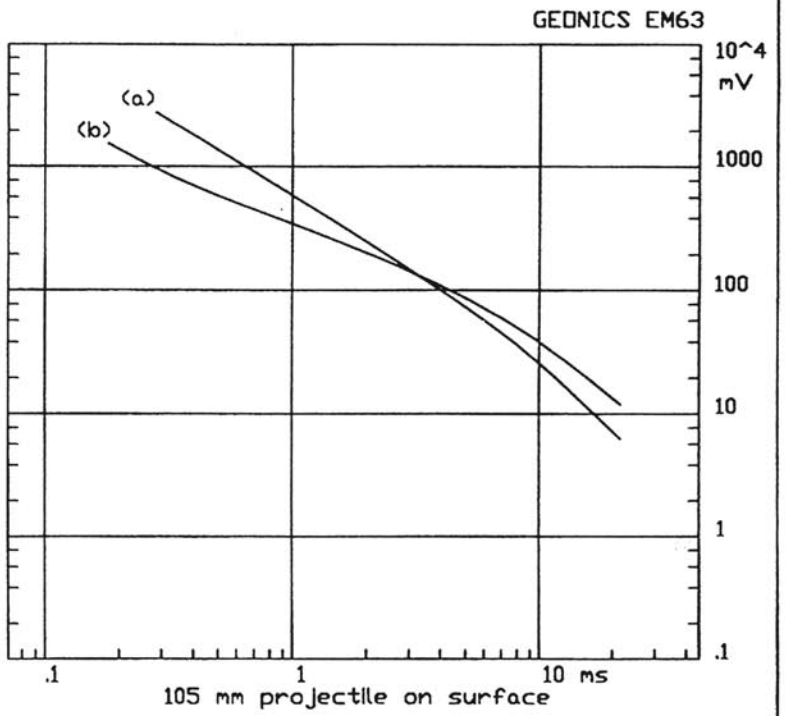

105 mm projectile on surface

Curve (a) - EM63 located directly over target
Curve (b) - EM63 removed a short distance along target main axis

Figure 11

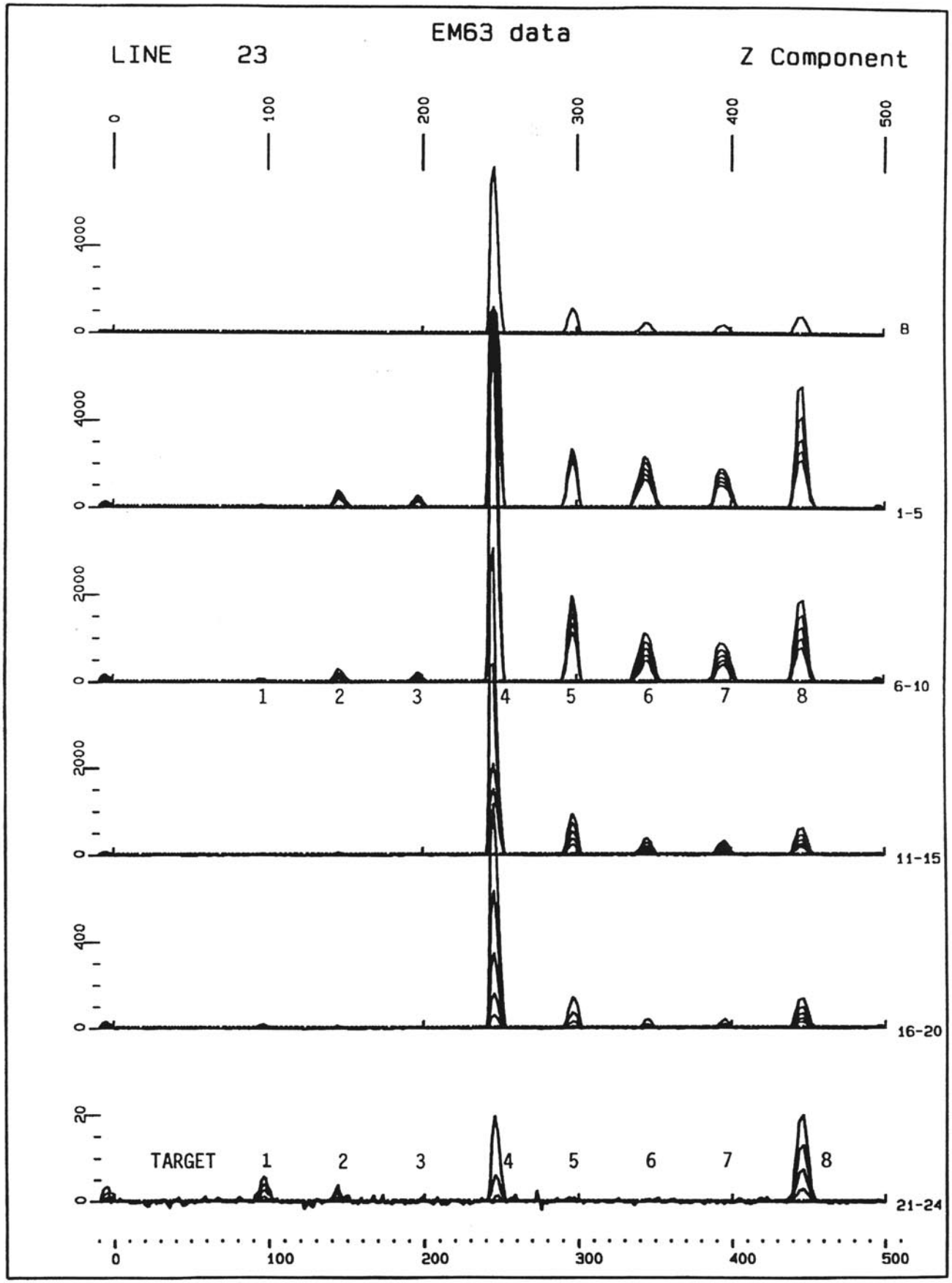
EM63 data
LINE 23
Z Component
0
100
200
300
400
500
4000
8
1-5
2000
1
2
3
4
5
6
7
8
6-10
11-15
400
16-20
20
TARGET
21-24

Figure 9

APPLICATION OF TIME DOMAIN ELECTROMAGNETIC TECHNIQUES TO UXO DETECTION

J.D. McNeill
Miro Bosnar
Geonics Limited
1745 Meyerside Drive, Unit 8
Mississauga, ON L5T 1C6
(905)670 9580

INTRODUCTION

This paper describes initial results of an investigation into the response from typical UXO targets to time domain electromagnetic (TDEM) systems such as the Geonics EM61; a principle objective is to learn the extent to which TDEM systems can distinguish between various types of UXO and scrap metal.

The paper consists of three parts. In Part I we describe the characteristics of the Geonics EM61 TDEM metal detector as background for later discussions on the nature of target response. A following paper (Hoekstra, P., these proceedings) describes survey data taken with an EM61 at various sites. In Part II we examine the theoretical response from a variety of metal objects (spheres, plates and pipes) selected on the basis of their resemblance to typical UXO targets or metallic scrap, to understand the main features of the response, and to determine what information can be derived from it. Finally, in Part III, we examine the response from actual UXO targets.

PART I

Fig. 1 shows schematically the coil configuration of an EM61. A transmitter coil, Tx, of dimensions 1x1 m, is close-coupled with the main receiver coil, Rx1, which is also 1x1 m. A subsidiary receiver coil, Rx2, parallel with these two coils, is located 0.4 m above them. The whole array is maintained a distance of 0.45 m above the ground, either by a pair of wheels, or optionally, by an operator harness.

The function of Rx2 is two-fold: firstly having suitably adjusting its turns-area beforehand, one can subtract the output signal of Rx2 from Rx1 to substantially reduce the response from near-surface targets compared with deeper targets. Secondly, the relative signal output from the two receiver coils is compared to determine the depth to small targets (i.e. targets whose dimensions are small compared with the 1 m side length of the various coils). Since the output of Rx2 is not used for signal analysis its presence will be ignored for the remainder of the paper.

The EM61 system waveforms are shown in Fig. 2. The transmitter current initially rises exponentially to a constant value, after which it is rapidly terminated in a linear ramp, of time-duration *to*. This transmitter current causes a relatively large primary magnetic field to intercept a potential target, as shown in Fig. 1. The magnetic field is linearly proportional to the transmitter current, so that terminating the current induces, as a result of Faraday's law, a voltage in the target, which, in turn, causes current to flow in the target. This current generates a secondary magnetic field, which is sensed (along with the much larger primary field) by the two receiver coils to detect the target. From the figure we observe that, in fact, target current is induced both when the transmitter current starts and stops. Since the primary magnetic field is much larger than the secondary field, measurement is made of the target transient response only during those periods of time when the transmitter current is zero.

As shown in Fig. 2 the target current, once initiated by the transmitter turn-off, is always a monotonically decaying waveform, the maximum amplitude of which is affected by target size, shape, depth, and position relative to the coil system. The duration of the transient current is determined by target dimensions and position relative to the coil system, target electrical conductivity and target magnetic permeability. In the conventional EM61, which was designed as a simple but effective metal detector, presence of a target is detected by simply opening a time gate in the receiver 400 microseconds after transmitter current turn-off, integrating the time response over the next 400 microseconds, and closing the gate. Such a technique obviously ignores much of the information contained in the decaying current, and in this paper we will assume that the transient response is now well defined by making the measurement with a large number of narrow

time gates during the entire duration of the transient response, so that we can use the characteristics of the decaying current for subsequent analysis.

Two further points concern the material which follows. The transmitter current waveform shown in Fig. 2 is periodic, with turnoff time *to*, which somewhat modifies the target response. To avoid this complication we assume that the transmitter current waveform turn-off is a step-function with turn-off of zero time duration, as shown in Fig. 3; we will be interested in details of the time response for $t>0$. Finally, the output of the receiver coil is actually proportional to the time rate of change of the secondary magnetic field, $dB(t)/dt$, rather than to the amplitude of the secondary magnetic field, $B(t)$. The latter, being directly related to actual current flow in the target, is more useful for analysis. Fortunately it can be easily obtained, for any time t, by integrating backwards up the decay curve of $dB(t)/dt$ from $t=\infty$ to $t=t$. All calculations and measurements described in this paper will thus be of $B(t)$. All measurements were made with a Geonics TEM47 transmitter and PROTEM receiver.

PART II

In this section we examine the theoretical and measured response from three model types, selected to approximate the behaviour of both various types of UXO and trash metal. The models are a sphere, a plate, and a cylinder. Several assumptions will be made in calculating their response.

(1) It will be assumed that the response of a target buried in the ground will be essentially that of the same target in air: that is, it is assumed that there are no significant interaction effects between the target and the ground, which always has finite conductivity and often has magnetic permeability slightly larger than that of free-space. The validity of this assumption is based on the fact that the conductivity of metallic targets is always at least six orders of magnitude greater than that of the ground, and, when all is said and done, virtually all UXO targets are ferrous, with relative permeability much greater (probably by at least a factor of fifty) than the ground.

(2) It will also be assumed, to simplify the calculations, that the targets are located at sufficient distance beneath the transmitter so that the primary magnetic field can be described as being uniform in the vicinity of the target. Thus we will be interested in the dipole response of our targets.

(3) The influence of displacement currents will be ignored, justified by the magnitude of the physical parameters of typical targets, and the relatively long times at which our measurements will be made.

Sphere Response

Our first target model of interest will be a sphere, which can represent an item of UXO but more probably will represent a fragment of exploded ordnance. Its chief advantage, otherwise, is that the response, which is relatively easily calculated, illustrates features which are the same for all metallic objects. With reference to Fig. 4a we assume that the sphere, initially assumed to have conductivity σ and relative permeability $K=1$ (with respect to free-space i.e. the sphere is non-ferrous), is located in a uniform, upwards directed, vertical magnetic field B_p, which is abruptly terminated at $t=0$. Immediately after primary magnetic field turn-off, eddy currents will flow on the surface of the sphere, distributed so as to maintain the magnetic field everywhere inside the sphere at the value which existed at the instant before turn-off. As indicated in Fig. 4a this current flow, which is circumferential, is maximum at the equator and zero at the poles. The magnitude of the initial current density is determined solely by the geometry of the target, and is independent of the electrical conductivity. Since however, the sphere has finite conductivity, the amplitude of the eddy currents starts to decay, causing a decaying magnetic field in the interior of the sphere, which, as a result of Faraday's law, will induce deeper circumferential currents to flow (Fig. 4b). They, too, will decay, in turn inducing deeper current flow. This behaviour repeats itself until eventually the currents become more or less uniformly distributed throughout the interior of the sphere, whereupon the current distribution no longer varies with time. At this point the entire current distribution, now stable, simply starts to decay exponentially with time, eventually decaying to zero.

Our interest lies in the external magnetic field produced by these varying currents. Somewhat surprisingly it can be shown that this field is exactly that which would be caused by a small magnetic dipole located at the sphere center and aligned parallel with, and in the same direction as the primary field. The magnitude of this dipole, which is a function of time, can be expressed as

$$m(t)=2\pi a^3 B_p f c(t) \qquad (1)$$

where B_p = primary magnetic field at the sphere center,
a = sphere radius,

and the function $fc(t)$, shown in Fig. 5, describes all aspects of the time behaviour of the secondary magnetic field.

What can be learned from this equation? We note that if, since $fc(0)=1$, we can measure the sphere response at very early time we obtain the product a^3B_p, and since we have a way of determining the target depth (using the second receiver coil) and thus B_p, we can determine a, the sphere radius directly.

The function $fc(t)$ can be broken into three time ranges; early time, where $fc(t)$ is approximately unity (allowing us to determine a), intermediate time, about which more will be said later, and late time, at which the response becomes exponential with time, having the form $\exp(-t/T)$ where T is the characteristic time-constant of the sphere. This time-constant T is given by

$$T=\mu_o\sigma a^2/\pi^2 \qquad (2)$$

where μ_o = permeability of free-space
and σ = sphere conductivity.

We see that, having obtained a as discussed above, measurement of T allows us to calculate σ, the sphere conductivity. We have now completely defined the sphere, illustrating the power of the time-domain electromagnetic method to diagnose useful properties of conductive targets.

A further feature of the sphere response is of interest. It was stated above that the induced dipole was parallel with the primary magnetic field. As our EM61 passes over a spherical target, the direction of the primary magnetic field, and thus of the induced magnetic dipole, varies continuously with instrument location, resulting in a survey profile that is always symmetrical along the survey line.

Suppose now that we allow the sphere to be ferrous, i.e. that the magnetic permeability is no longer unity (typical values of K for iron and steel are in the range 50-200). This change has three effects on the function $fc(t)$, as shown in Fig. 6. The first is that $fc(0)$ is now a slowly varying function of K. This need not concern us, since for the range of K given above, $fc(0)\approx 3$, and we can still determine the sphere radius to reasonable accuracy. The second effect is that the intermediate zone mentioned above becomes extended in time by an amount dependent on K, and during this intermediate time $fc(t)$ now decays as $t^{1/2}$. Thirdly, once again at late time the response again becomes exponential, but now with late-stage time constant T given by

$$T=\frac{4}{9}K\frac{\mu_o\sigma a^2}{\pi^2} \qquad (3)$$

The effect of the large value of K will be to greatly increase the late-stage time constant, but note that this will be partly offset by the fact that the conductivity of ferrous metals is usually about a factor of ten less than typical non-ferrous metals.

In the material that follows we will see that the time behaviour of normal eddy current flow in all metallic bodies resembles that of the sphere. At early time the currents flow around the edge of the body, distributed in such a fashion as to keep either the internal magnetic flux or the magnetic field itself at the value that existed before primary magnetic field turn-off. At this time, measurement of the response gives useful geometrical information about the body, independent of its conductivity, but (usually weakly) dependent on its magnetic permeability. During intermediate time, the duration of which depends on K, the eddy currents decay and, at the same time alter their spatial distribution. At late time, the current distribution stabilizes, and the effective inductance and resistance of each current loop no longer vary with time; during this stage the decay becomes exponential, with a simple time-constant which is determined by the conductivity, relative permeability, and target geometry and size. We see that all stages of the response will give useful information about the target.

The characteristics of the intermediate range appear to be of particular interest, and to make this region easier to analyze (by reducing the effect of the late stage exponential decay), we have adopted the practice of transforming the data by normalizing with respect to the late stage behaviour. We do this by successively dividing the measured or calculated time function, $fm(t)$ or $fc(t)$ respectively, by the function $e(t)= A\ exp(-t/T1)$, where $T1$ is adjusted until the late-stage behaviour is no longer a function of time; this value of $T1$ is therefore

T, the late-stage time constant. The value of A is then adjusted until the (non time-varying) late-stage response has the value unity. The function $ft(t)=fm(t)/e(t)$ or $ft(t)=fc(t)/e(t)$, called the transformed time-response, is used to analyze the intermediate stage behaviour.

This procedure is illustrated in Fig. 7a, where the calculated data of Fig. 5 have been transformed, resulting in a value for $T1=T$ of 2.9 msec. The two regions of the curve (intermediate and late stage) are now well separated. Furthermore replotting the transformed data as a function of t/T, as shown in Fig. 7b, clearly shows that, for a conductive sphere with $K=1$, the late stage commences at $t\sim T$. The same procedure was carried out on the ferrous spheres of Fig. 6; the results are shown in Fig. 8. It will be observed that, as long as $K>50$, the intermediate stage behaviour for all ferrous spheres is identical, decaying as $t^{1/2}$, and that late stage is now reached at $t/T\sim 1.5$.

In the remainder of this paper we will show several measured curves of $fm(t)$ for a variety of metallic objects. Since we are primarily interested in the relative time response of the different targets, values of $fm(t)$ are given in arbitrary units and are not necessarily consistent from graph to graph. Figs. 9a, b show such data for two conductive spheres (non-ferrous and ferrous respectively). The agreement with theory is excellent.

Plate Response

Our next target model, a small thin plate, will most probably represent either a fragment of exploded ordnance or a piece of scrap metal. The data of Fig. 10 show $f(t)$ for both non-ferrous and ferrous (but otherwise similar) plates, with the primary magnetic field perpendicular to the plane of the plates. The two responses are very similar, the principle difference being that the ferrous plate shows a more steeply dipping intermediate stage decay, similar to that of the ferrous spheres. This response changes radically, however, when the direction of the primary magnetic field is altered to be parallel with the plane of the plates. In the case of the non-ferrous plate there will be virtually zero response, since the thin plate is in null-coupling with the primary magnetic field and no eddy currents are induced. There will also be no eddy current flow in the ferrous plate, but in this configuration the parallel primary magnetic field now polarizes the magnetic dipoles in the plate, causing them to line up with the primary magnetic field. When the primary field is abruptly terminated, the polarized dipoles do not return to random polarization immediately, and as they do randomize, they produce a strong, decaying secondary magnetic field, which at a distance will also resemble that of a decaying dipolar field. For the ferrous plate, when the primary magnetic field is perpendicular to the plate, polarization of the magnetic dipoles in the plate is minimal, and eddy current response predominates; when the primary magnetic field is parallel with the plate, polarization of the magnetic dipoles in the plate is optimized, and their decay dominates the response. This phenomenon is shown in Fig. 11a, from which it will be seen that at early and intermediate time the secondary magnetic field from the two types of response is almost equal; it is only at late time that the eddy current response dominates. Furthermore it is seen in Fig. 11b that, unlike the eddy current response, the polarization response never becomes exponential. In applying the transformation described above, no value of $T1$ allows the late-stage response to become invariant with time.

This phenomenon plays a very important role in the spatial response of ferrous plates, an example of which is shown in Fig. 12, which illustrates a short section of EM61 survey profile over a number of ferrous and non-ferrous objects located on the ground. As the EM61 approaches a ferrous plate, for example (b), the primary magnetic field is initially approximately parallel with the plane of the plate, and thus induces strong polarization response, with its characteristic decay. As the EM61 moves directly over the plate, excitation of polarization response ceases, to be supplanted by strong eddy current response, with different decay characteristics. As the EM61 moves on, once again polarization response dominates. The net effect of these two different responses is (a) to greatly broaden the spatial response of the plate, compared with other target types, for example aluminum plate (a), and (b) to complicate the time behaviour of the response compared with other target types. Both of these features are of great use in identifying responses from a ferrous plate. It is interesting to note that the close-coupled, horizontal coil configuration of the EM61 is ideal for identifying plate responses. The polarization response described above also occurs in the frequency domain (causing a strong quadrature phase response from null-coupled steel plates) which, because of the relatively large intercoil spacing used in devices such as the Geonics EM31, makes interpretation of such combined eddy current/polarization responses extremely difficult.

Cylindrical Shell Response

Our final target model, short sections of steel pipe, will most likely resemble UXO. We note that, like the plate

and unlike the sphere, we will have to examine the responses when the primary magnetic field is both perpendicular and parallel to the shell axis.

Before examining the time response of cylindrical shells it is necessary to digress to study the nature of the magnetostatic response of our different ferrous targets. Fig. 13 illustrates schematically the effect of placing each ferrous target in a uniform (static) magnetic field (note that placing a non-ferrous target of any shape in this field would cause no deformation of the field). The ferrous plate causes a small deformation of the uniform field, slightly increasing the magnetic flux that intercepts the plate. Recall that, when we shut off the magnetic field, the initial current that flows in the plate will just be enough to balance out this flux, and thus, as a result of flux-gathering, the initial secondary magnetic field from the ferrous plate will be somewhat larger than that from an identical non-ferrous plate, as seen in Fig. 13. This effect will be about the same for a ferrous sphere, or for a ferrous cylinder perpendicular to the primagnetic field, but if we orient a long ferrous cylinder parallel to the primary magnetic field, the flux-gathering is substantial, and we thus expect that the initial response from a ferrous cylinder (or cylindrical shell) oriented parallel to the primary magnetic field will be much larger than from the same cylinder perpendicular to the field.

Fig. 14 shows the response from one of the steel pipes with both orientations of the primary magnetic field. The effect described above is immediately noticeable. However another effect is also evident; during the intermediate time the decay rate, when the shell axis is parallel to the primary field, is much more gradual than when perpendicular. This appears to be due to the fact that the transient secondary magnetic field is now being caused both by decaying eddy currents and decaying polarization, the effects of which are additive.

PART III

We now examine the time response from a series of five pieces of UXO. These consist of (a) a 40 mm shell, (b) a 60 mm M2 mortar round, (c) an 81 mm mortar round, (d) a 105 mm M14 shell, and (5) a 155 mm M107 shell.

Note that these items most nearly resemble our cylindrical steel pipes, but that they have different dimensions (both length and diameter), and also differ in that they have pointed noses and in some cases taper down to small tail assemblies.

Results from the individual shells are shown in Figs. 15a-e, where we note that, in all cases where the primary magnetic field is parallel rather than perpendicular to the shell axis, thus inducing solenoidal current flow, (a) the early stage response is greater, (b) the intermediate stage decays more slowly, and (c) the late-stage time constant is larger. These are significant differences since, in general, the axis of such a shell will lie at an arbitrary angle with respect to the direction of the primary magnetic field, which will therefore have components both parallel and perpendicular to the shell axis. Both components will excite the appropriate eddy current flow, but if measurement of the total response is made out to sufficiently late time, in nearly all cases the limiting response will be caused by solenoidal current flow. Measurement of the various spatial components of the response will then yield the orientation of the shell (note that for this type of anomaly the profile will generally be asymmetrical along the survey line). Furthermore, the late-stage time-constant may be reasonably specific to a given shell since it will depend on, amongst other factors such as steel permeability and conductivity, the internal structure of the shell, specifically to different variations of shell wall-thickness.

Finally, Fig. 16 shows detailed behaviour of the intermediate time response for each of the shells, as exemplified by the transformed time responses. It is noted that this response is quite different for the various shell types. Once the orientation of the shell has been established from the late stage measurements, the intermediate time response can be separated out, and this feature too may well prove to be diagnostic.

Conclusions

It is probably unlikely that, in a blind test, a TDEM survey would be able to specify the nature of subsurface targets sufficiently well to identify different types of UXO. Furthermore our measurements have only been of UXO that was cylindrical by nature. Nevertheless, given "a priori" knowledge of the decay characteristics of UXO that are expected in a survey area (specifically, the value of $fm(0)$, the nature of the intermediate time behaviour, and the value of the late-stage time-constant), the evidence presented in this paper suggests that it might be possible to separate out various types of UXO (a) from each other and (b) from exploded ordnance and other trash metal. Further measurements are certainly necessary to confirm the extent of this possible uniqueness. At the least it would appear that the TDEM technique offers more promise for identification of UXO

than techniques based on potential field theory.

Acknowledgements

Measurement of the decay characteristics of the UXO were carried out under contract to Defense Research Establishment Suffield, who also supplied the dummy rounds.

Bibliography

Hoekstra, P. 1996. "Time Domain Electromagnetic Metal Detectors" Proceedings, UXO Forum 1996.

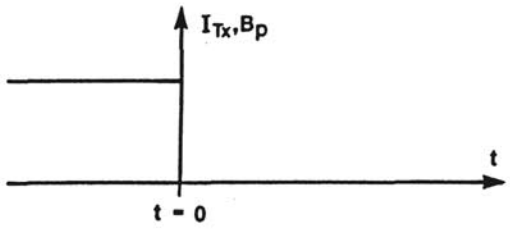

Fig. 3 Step function current

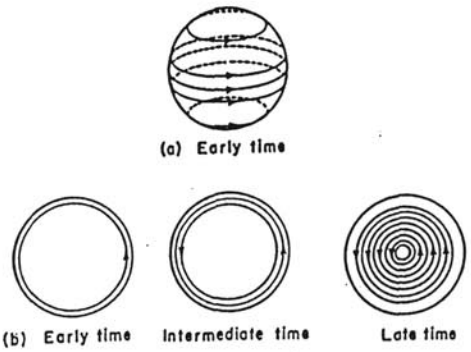

Fig. 4 Decaying sphere currents

FIGURES

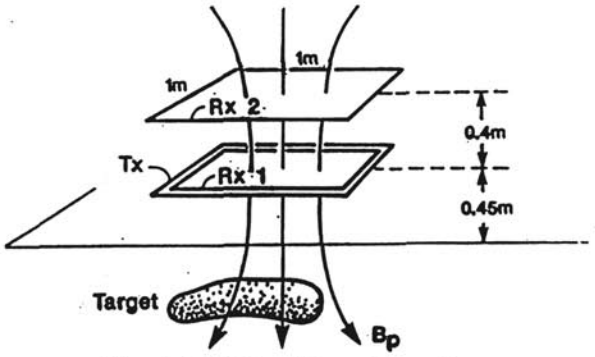

Fig. 1 EM 61 coil configuration

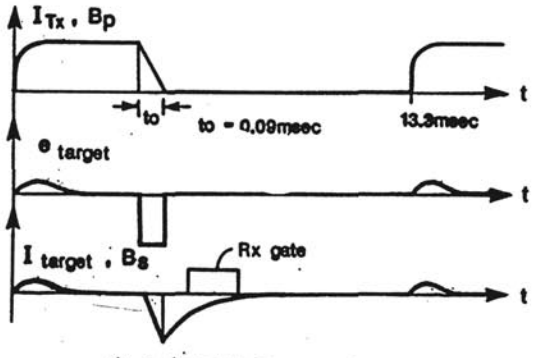

Fig. 2 EM 61 waveforms

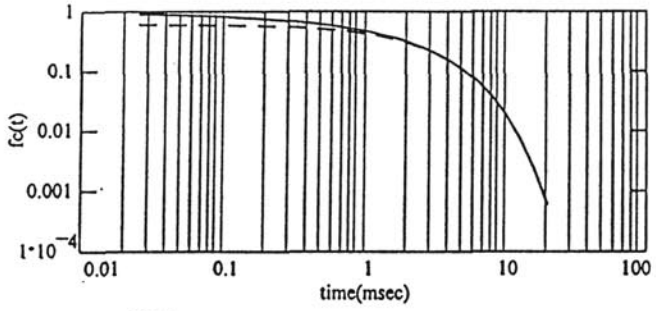

— fc(t)
— best-fit exponential)

Fig. 5 Non-ferrous sphere response

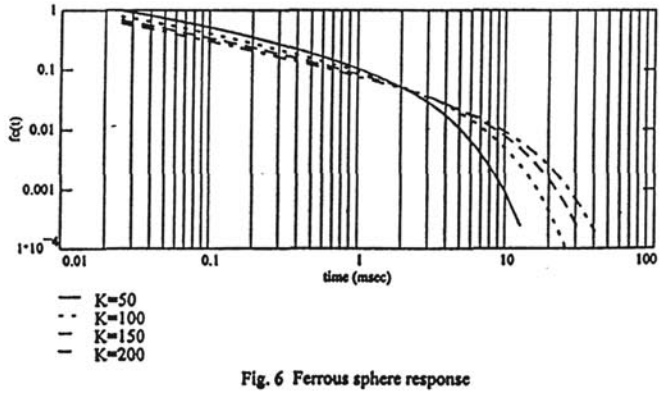

Fig. 6 Ferrous sphere response

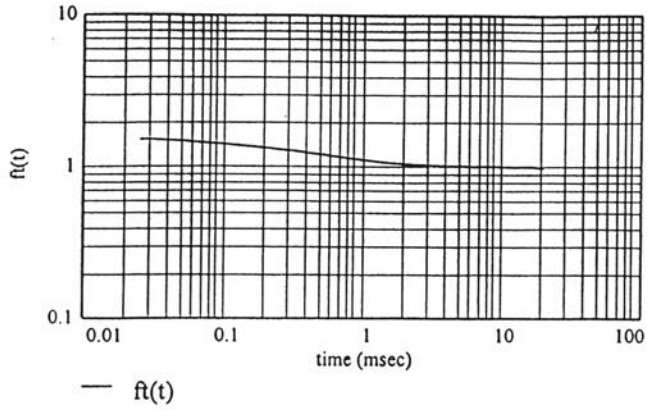

Fig. 7a Transformed response

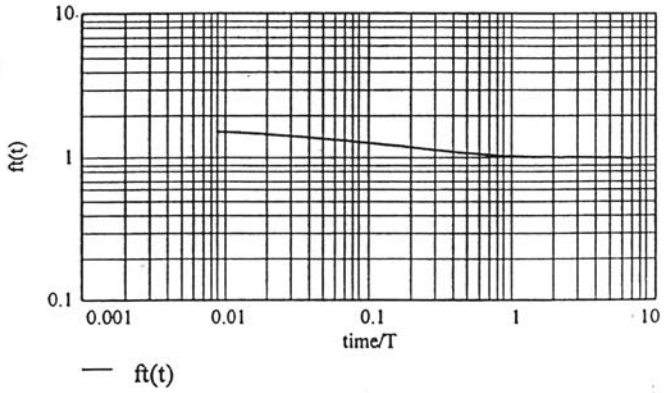

Fig. 7b Transformed response

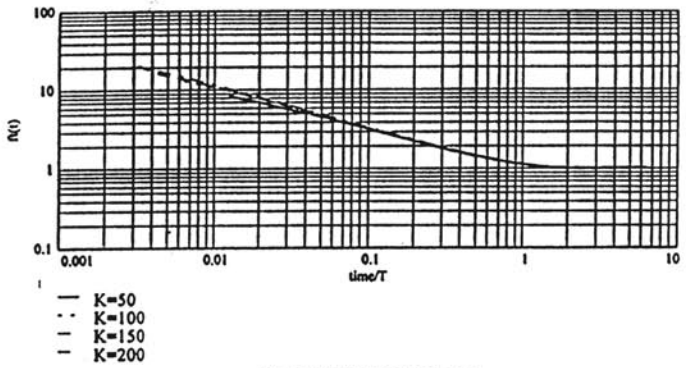

Fig. 8 Transformed response

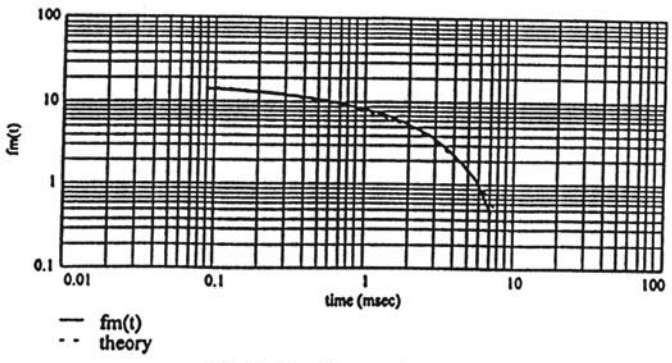

Fig. 9a Non-ferrous sphere response

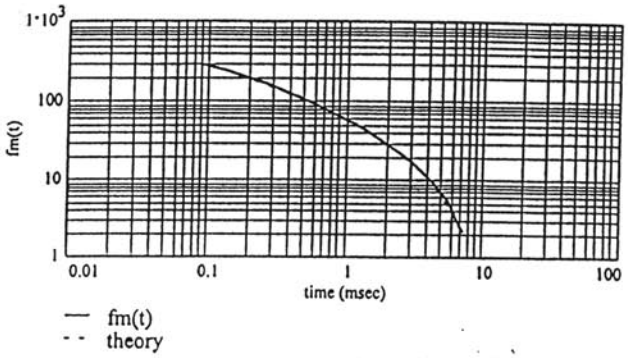

Fig. 9b Ferrous sphere response

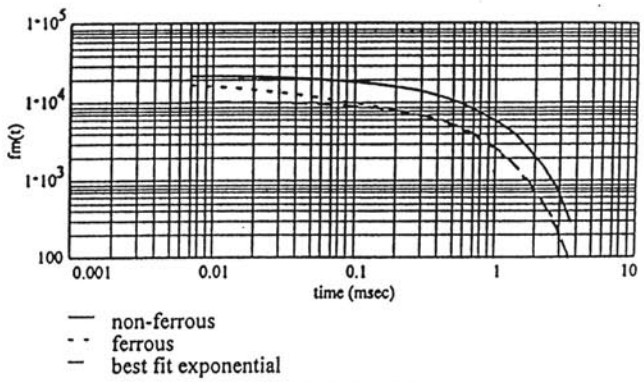

Fig. 10 Plate response

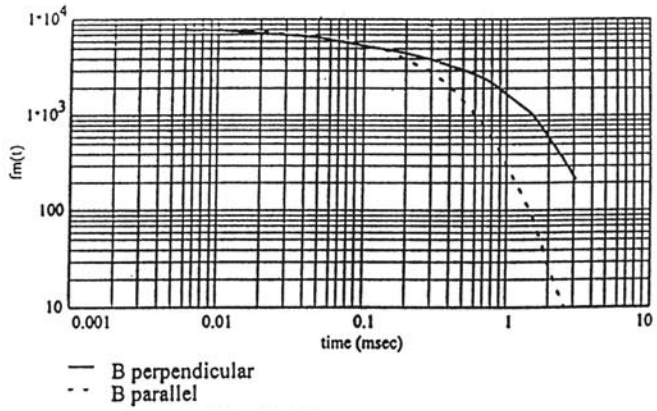

Fig. 11a Plate response

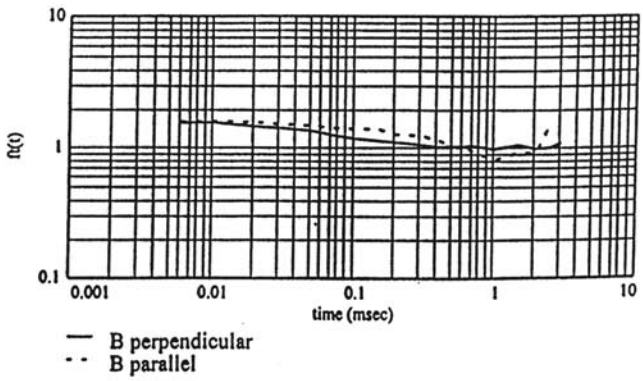

Fig. 11b Transformed response

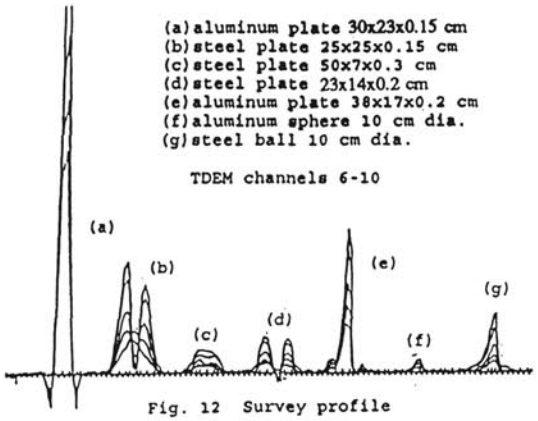

Fig. 12 Survey profile

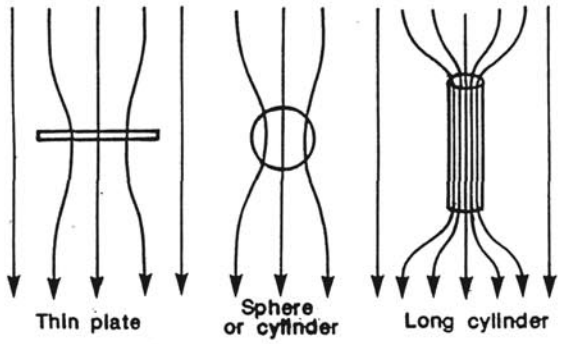

Fig. 13 Flux gathering

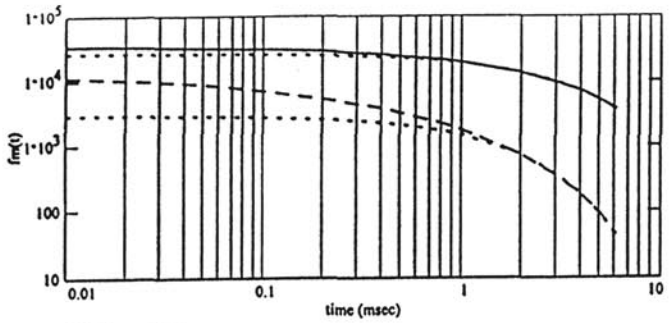

Fig. 14a Pipe response

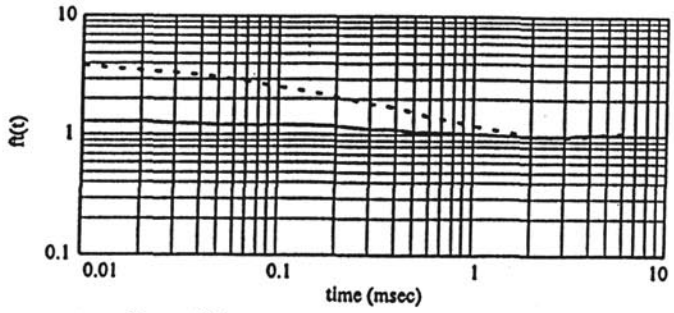

Fig. 14b Transformed response

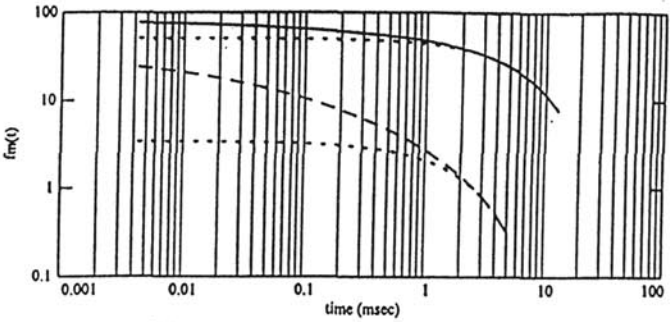

Fig. 15a 40mm shell response

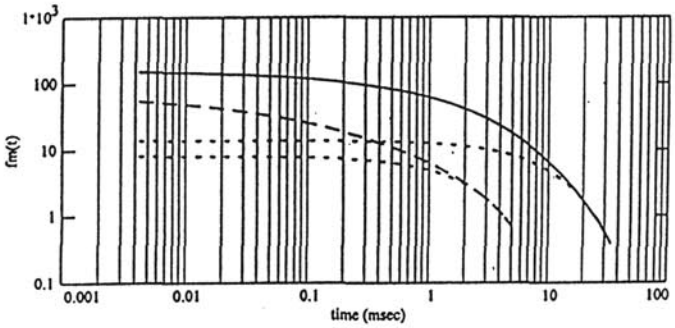

Fig. 15b 60mm M2 mortar response

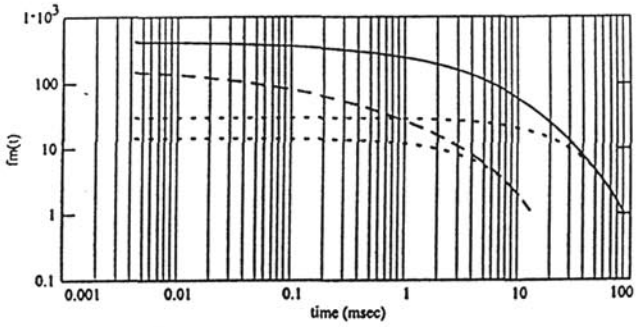

Fig. 15c 81mm mortar response

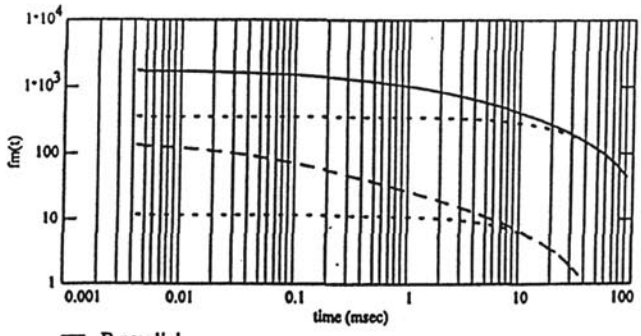

Fig. 15d 105mm M14 shell response

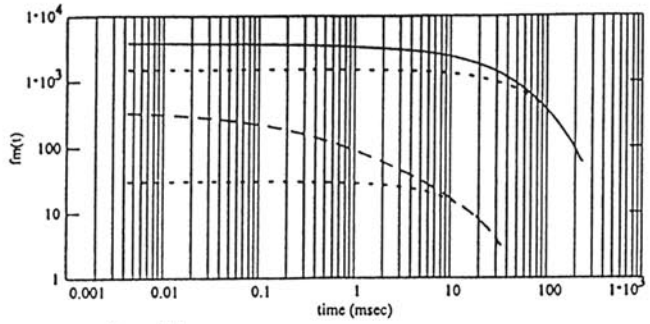

— B parallel
– B perpendicular
· · best fit exponential
· · best fit exponential

Fig. 15e 155mm M107 shell response

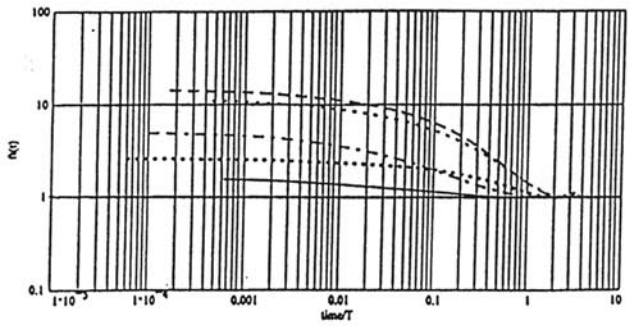

— 40 mm shell
· · 60 mm M2 mortar
– 81 mm mortar
– 105mm M14 shell
· · 155 mm M107 shell

Fig. 16 Transformed responses